A precursor-inducible zebrafish model of acute protoporphyria with hepatic protein aggregation and multiorganelle stress

Jared S. Elenbaas,[*,1] Dhiman Maitra,[*,1] Yang Liu,[†] Stephen I. Lentz,[‡] Bradley Nelson,[‡] Mark J. Hoenerhoff,[§] Jordan A. Shavit,[†] and M. Bishr Omary[*,‡,¶,2]

[*]Department of Molecular and Integrative Physiology, [†]Department of Pediatrics and Communicable Diseases, Division of Pediatric Hematology and Oncology, [‡]Department of Internal Medicine, and [§]In-Vivo Animal Core, Unit for Laboratory Animal Medicine, University of Michigan, Ann Arbor, Michigan, USA; and [¶]Veterans Affairs Ann Arbor Healthcare System, Ann Arbor, Michigan, USA

ABSTRACT **Protoporphyria is a metabolic disease that causes excess production of protoporphyrin IX (PP-IX), the final biosynthetic precursor to heme. Hepatic PP-IX accumulation may lead to end-stage liver disease. We tested the hypothesis that systemic administration of porphyrin precursors to zebrafish larvae results in protoporphyrin accumulation and a reproducible nongenetic porphyria model. Retro-orbital infusion of PP-IX or the iron chelator deferoxamine mesylate (DFO), with the first committed heme precursor α-aminolevulinic acid (ALA), generates high levels of PP-IX in zebrafish larvae. Exogenously infused or endogenously produced PP-IX accumulates preferentially in the liver of zebrafish larvae and peaks 1 to 3 d after infusion. Similar to patients with protoporphyria, PP-IX is excreted through the biliary system. Porphyrin accumulation in zebrafish liver causes multiorganelle protein aggregation as determined by mass spectrometry and immunoblotting. Endoplasmic reticulum stress and induction of autophagy were noted in zebrafish larvae and corroborated in 2 mouse models of protoporphyria. Furthermore, electron microscopy of zebrafish livers from larvae administered ALA + DFO showed hepatocyte autophagosomes, nuclear membrane ruffling, and porphyrin-containing vacuoles with endoplasmic reticulum distortion. In conclusion, systemic administration of the heme precursors PP-IX or ALA + DFO into zebrafish larvae provides a new model of acute protoporphyria with consequent hepatocyte protein aggregation and proteotoxic multiorganelle alterations and stress.—Elenbaas, J. S., Maitra, D., Liu, Y., Lentz, S. I., Nelson, B., Hoenerhoff, M. J., Shavit, J. A., Omary, M. B. A precursor-inducible zebrafish model of acute protoporphyria with hepatic protein aggregation and multiorganelle stress. *FASEB J.* 30, 1798–1810 (2016). www.fasebj.org**

Key Words: autophagy · endoplasmic reticulum stress · protoporphyrin IX · unfolded protein response

Porphyrias are metabolic disorders that arise from imbalance in the heme biosynthesis pathway, often from a mutation affecting an enzyme involved in heme synthesis. The porphyrias are categorized as hepatic or erythropoietic, depending on the tissue that generates the excess porphyrins, and as either acute or cutaneous, depending on the disease presentation (1). Protoporphyria is a cutaneous erythropoietic porphyria that is subdivided into erythropoietic protoporphyria (EPP) and X-linked protoporphyria (XLP). Both diseases are characterized by elevated levels of circulating protoporphyrin IX (PP-IX) (2–4), the last precursor in the heme biosynthetic pathway.

Ferrochelatase (FECH) is the enzyme responsible for metabolizing heme from PP-IX and iron (5) and is the most frequently mutated enzyme in protoporphyria, with approximately 95% of patients having reduced FECH activity, resulting in EPP (6–8). Mutation of FECH may result in EPP; while approximately 2% of patients with protoporphyria develop XLP because of a gain of function mutation in ALAS2 (9), the enzyme that catalyzes the production of α-aminolevulinic acid (ALA, the first committed precursor in the pathway) from glycine and succinyl-CoA (10). In both EPP and XLP, PP-IX accumulates in tissues such as blood, skin, and especially the liver (2), with hepatic PP-IX levels increasing by over 20,000-fold compared with normal levels (11). Hepatic manifestations of protoporphyria are observed in less than 5% of patients (2), but up to 25% of patients may present with cholestasis (11, 12). Patients with XLP or biallelic *FECH* mutations have a greater risk of developing liver complications (8). The incomplete penetrance of protoporphyria in different

Abbreviations: ALA, α-aminolevulinic acid; DDC, 3,5-dicarbethoxy-1,4-dihydrocollidine; DFO, deferoxamine mesylate; eGFP, eukaryotic green fluorescent protein; EPP, erythropoietic protoporphyria; ER, endoplasmic reticulum; FECH, ferrochelatase; MS, mass spectrometry; PDI, protein disulfide isomerase; PP-IX, protoporphyrin IX; SA, succinylacetone; UPR, unfolded protein response; XLP, X-linked protoporphyria

[1] These authors contributed equally to this study.

[2] Correspondence: University of Michigan Medical School, Department of Molecular and Integrative Physiology, 7744 Medical Science Bldg. II, 1137 Catherine St., Ann Arbor, MI 48109-5622, USA. E-mail: mbishr@med.umich.edu

doi: 10.1096/fj.201500111R

This article includes supplemental data. Please visit *http://www.fasebj.org* to obtain this information.

families (13, 14) suggests the existence of undiscovered genetic modifiers.

Porphyrins cause hepatic protein aggregation of the nuclear lamins and the cytoplasmic keratin intermediate filament proteins (15). Protein aggregation of the intermediate filament cytoskeleton, in particular, is associated with several human diseases (16, 17). For example, human and mouse hepatocytes may develop and accumulate Mallory-Denk bodies, which consist of intracellular protein aggregates comprising mostly keratins, as a result of several molecular alterations, including transamidation of keratins (18, 19). In mice, long-term ingestion of porphyrinogenic toxins such as 5-diethoxycarbonyl-1,4-dihydrocollidine (DDC) also leads to Mallory-Denk body formation (20). In addition to the phototoxicity of porphyrins, oxidative stress also occurs in the absence of light. For example, treating cultured cells with PP-IX increases intracellular levels of H_2O_2 (21–23). In addition, porphyrins have been reported to generate electron-rich anion radicals by a microsomal enzymatic system without light activation (24, 25). The mechanism by which porphyrins increase oxidative stress and cause protein aggregation is unclear, as are the effects of protein aggregation on disease etiology in the context of porphyrias.

The endoplasmic reticulum (ER) serves as the major site of protein folding and refolding in the cell. A greater load of unfolded or aggregated proteins than the ER has the capacity to refold may cause ER stress (26). In cases of ER stress, the unfolded protein response (UPR) may be activated (27). The UPR is an adaptive response to ER stress and may induce degradation of misfolded or unfolded proteins by autophagy and other pathways (27). ER stress is associated with a plethora of diseases (28, 29), but its role in porphyria-induced damage is unclear.

Genetic models of EPP (30), variegate porphyria (31), and hepatoerythropoietic porphyria (32) have been generated in zebrafish, but their utility may be somewhat limited by the necessity to breed the recessive mutant alleles into new genetic backgrounds. Raising affected zebrafish to reproductive age also presents a challenge because the mutants display severe sensitivity to light. Given the genetic tractability and drug-screening potential of zebrafish to study liver diseases (33), an inducible model of protoporphyria provides a potentially powerful system to discover genetic modifiers and screen for therapeutic and exacerbating agents.

Here we present inducible zebrafish models of EPP and XLP by infusing heme precursors, which result in the accumulation of PP-IX in the liver of zebrafish larvae and consequent hepatic stress. These techniques may be adapted to develop additional inducible porphyria models by infusing agents that inhibit different steps of the heme biosynthesis pathway or various heme precursors. Inducible manipulation of the heme biosynthetic pathway provides an important adjunct to the zebrafish porphyria models to improve our understanding of the genetic and molecular aspects of porphyrias *in vivo*.

MATERIALS AND METHODS

Fish lines and husbandry, and mice

All fish experiments were conducted using wild-type zebrafish (*Danio rerio*) larvae from a cross of AB and TL adult zebrafish (ABTL) or transgenic ABTL zebrafish with eukaryotic green fluorescent protein (eGFP)-tagged fibrinogen β [A19 line (34)]. It is noteworthy that the expression of eGFP in A19 larvae is liver specific (34). Transgenic *FECH* (3–5 mo old) and DDC-fed (5 d, 0.1% DDC) mice were used as described previously (15, 35). Animal care guidelines were followed as approved by the University of Michigan Animal Care and Use Committee and per recommendations in the *Guide for the Care and Use of Laboratory Animals* from the National Institutes of Health (Bethesda, MD, USA).

Infusions, drug treatments, and lysosome staining

Zebrafish larvae were retro-orbitally infused with approximately 2 nl of the indicated solution at the indicated time before analysis. Control larvae were infused with carrier (DMSO for PP-IX infusions and H_2O otherwise). After infusion, larvae were placed in a dark incubator for the indicated times. Infused PP-IX (1 mg/ml) was prepared in DMSO from a 10 mg/ml stock solution in *N,N*-dimethylacetamide; deferoxamine mesylate (DFO), 5-aminolevulinic acid hydrochloride (ALA) and succinylacetone (SA) were prepared in H_2O at final concentrations of 50, 50, and 25 mg/ml, respectively. All chemicals were obtained from Sigma-Aldrich (St. Louis, MO, USA). Zebrafish larvae were treated with a 100-fold dilution of LysoTracker Yellow HCK-123 (Life Technologies, Carlsbad, CA, USA) for 1 h and were washed twice, microdissected in PBS, mounted in glycerol, and imaged with a Zeiss AXIO Imager.M2 (Carl Zeiss, Oberkochen, Germany) with Texas Red and LysoTracker Yellow HCK-123 channels. The number of puncta per liver was counted and classified as low (0–10), medium (11–50), or high (>50). A χ^2 test was used to determine statistical significance (n = 13–17).

Transcriptional analysis

Six days after fertilization, A19 larvae were anesthetized and microdissected in PBS using 29-gauge insulin syringes after the indicated hours after infusion. Livers (12–20 per condition) were collected and pipetted into chilled RNAlater (Life Technologies), followed by RNA extraction using Qiagen RNeasy micro or microplus kits (Qiagen, Venlo, Limburg, Netherlands). The RNA concentration was determined using NanoDrop (Thermo Fisher Scientific, Waltham, MA, USA), and cDNA was reverse-transcribed using the TaqMan Reverse Transcription Kit (Life Technologies). Quantitative PCR was performed using Eppendorf realplex^2 (Eppendorf, Hamburg, Germany) and SYBR Green Supermix (Bio-Rad Laboratories, Hercules, CA, USA) with the primers (36, 37) listed in Table 1. Two independent experiments were performed, each with 3 biologic replicates for the control and experimental groups per time point. The amplification of target genes was compared to the reference gene, *rppO* (37). Expression relative to control larvae was calculated by the $\Delta\Delta C_t$ method and reported with error bars representing SE. Significance was determined by Student's t test comparing the expression of control and experimental samples unique to each time point.

Immunoblotting, proteomic analysis, and porphyrin quantification

Dissected tissues were placed in chilled radioimmunoprecipitation assay buffer (Thermo Fisher Scientific) containing protease inhibitors and then homogenized by sonication. Samples were pelleted to remove insoluble material, and protein levels were determined using a bicinchoninic acid assay (Thermo Fisher

TABLE 1. *Study primers*

Transcript	Forward primer	Reverse primer
atf3	CTGTCCCAGAGGAGAACGAC	TGGTTCTTCAGCTCCTCGAT
atf4b1	TTAGCGATTGCTCCGATAGC	GCTGCGGTTTTATTCTGCTC
atf6	CTGTGGTGAAACCTCCACCT	CATGGTGACCACAGGAGATG
atg5	AGAGAGGCAGAACCCTACTATC	CCTCGTGTTCAAACCACATTTC
atg16l1	AATTCGTTCAGCTCGTCTCC	CAGCGTTCACTTCTCCATCA
becn	GATCATGCAATGGTGGCTTTC	CCTCCTGTGTCCTCAATCTTT
bip	AAGAGGCCGAAGAGAAGGAC	AGCAGCAGAGCCTCGAAATA
chop	AAGGAAAGTGCAGGAGCTGA	TCACGCTCTCCACAAGAAGA
perk	TGGGCTCTGAAGAGTTCGAT	TGTGAGCCTTCTCCGTCTTT
rpp0	CTGAACATCTCGCCCTTCTC	TAGCCGATCTGCAGACACAC
xbp1s	TGTTGCGAGACAAGACGA	CCTGCACCTGCTGCGGACT

Scientific). Samples were then dissolved in reducing Laemmli sample buffer and separated by SDS-PAGE. Proteins were transferred to Immobilon-P Membranes (EMD Millipore, Darmstadt, Germany), followed by immunoblotting and visualization by chemiluminescence (Thermo Fisher Scientific). Antibodies were obtained from Santa Cruz Biotechnology (Dallas, TX, USA) (mouse anti-ubiquitin, rabbit anti-ATF4), Abcam (Cambridge, MA, USA) (rabbit anti-lamin B1), Aviva Systems Biology (San Diego, CA, USA) (rabbit anti-protein disulfide isomerase [PDI]), and Cell Signaling (Danvers, MA, USA) (mouse anti-CHOP, rabbit anti-LC3B). Equal loading was confirmed using Ponceau S staining (Sigma-Aldrich). For mass spectrometry (MS) analysis, a gradient SDS–polyacrylamide gel (after protein separation under reducing conditions) was stained with Coomassie Blue dye, and the high-molecular-weight regions of the gel were excised from lanes containing control and ALA + DFO–infused larval liver protein homogenates. Gel strips were digested with trypsin, then analyzed by MS. Aggregated proteins were defined as the polypeptides that were detected >150 kDa but have a known monomeric molecular mass of <125 kDa, and were found in the treated but not the control samples. Porphyrin quantification was described previously (35).

Histology and transmission electron microscopy

Larvae were anesthetized as described previously (38) and placed in 4% buffered paraformaldehyde. Larvae were mounted in Histogel (Thermo Fisher Scientific), embedded in paraffin, cut into 4 μm sections, and stained with hematoxylin and eosin. For ultrastructural analysis, larvae at 4 days after fertilization were infused on 2 consecutive days with H_2O or ALA + DFO, anesthetized, and fixed for 2 h in 2% paraformaldehyde and 2% glutaraldehyde in PBS. After two 10 min washes in PBS, larvae were postfixed in 1% osmium tetroxide for 45 min. The samples were dehydrated though a graded ethanol series and mounted in propylene oxide. Samples were infiltrated with increasing ratios of EPON (Miller-Stephenson Chemical, Danbury, CT, USA) to propylene oxide as follows: 1:3, 1:1, 3:1, 1:0. Larvae were then embedded in flat molds. Sections were made with a Leica EM UC7 ultramicrotome (Leica Camera, Wetzlar, Germany), stained for 10 min with 5% aqueous uranyl acetate, washed, stained with lead citrate, and examined with a JEOL JEM 1400 plus transmission electron microscope (JEOL USA, Peabody, MA, USA).

Imaging of zebrafish livers and histologic sections

Zebrafish livers were microdissected, mounted in glycerol, and imaged with a Zeiss Axio Imager.M2 (Texas Red and eGFP filters). Fluorescence intensity was determined using ImageJ software (Image Processing and Analysis in Java; U.S. National Institutes of Health). Polarization microscopy was used to visualize birefringence of hepatic pigment deposits. Zebrafish larvae tissue sections were illuminated with polarized and brightfield light on a Leica BM6000 microscope. White balanced images were captured with a ×63 [1.2 numerical aperture (N.A.)] water immersion objective and a Leica DFC450C 5-megapixel CCD color camera.

Confocal microscopy of live zebrafish

Zebrafish were anesthetized with tricaine and immobilized in 0.8% low-melting-point agarose. An Olympus Fluoview 500 laser scanning confocal microscope (Olympus, Tokyo, Japan) was used to capture z-series through the liver with a ×10 (0.4 N.A.) objective. eGFP was visualized by excitation with a 488 nm argon laser and emissions between 505 and 525 nm, and PP-IX was visualized by excitation with a 405-nm laser diode and emissions above 560 nm.

RESULTS

PP-IX accumulates in livers of larvae infused with PP-IX or coinfused with ALA and DFO

Models for EPP and XLP were generated by retro-orbital infusion of PP-IX alone or a combination of ALA and DFO. DFO is a potent iron chelator that prevents the insertion of iron into the PP-IX ring, while ALA is the first committed precursor in the heme biosynthesis pathway. Similar to patients with protoporphyria and other porphyria animal models, fluorescent porphyrins accumulated in the livers of larvae infused with PP-IX or ALA + DFO but not in larvae infused with the carriers DMSO or H_2O (**Fig. 1*A***). Larvae exposed to light had a high rate of mortality and therefore were shielded from light after infusion in all subsequent experiments. Accumulation of fluorescent porphyrins was observed as early as 5 h after infusion and was observed in other tissues, including neural and endothelial tissues (Fig. 1*A*). The intestine was also brightly fluorescent in larvae infused with PP-IX and ALA + DFO (Fig. 1*Ab′*, *c′*) but to a much lesser extent in larvae infused with DMSO (Fig. 1*Aa′*). We focused on the ALA + DFO model in the remainder of our studies because it provided a more robust and consistent

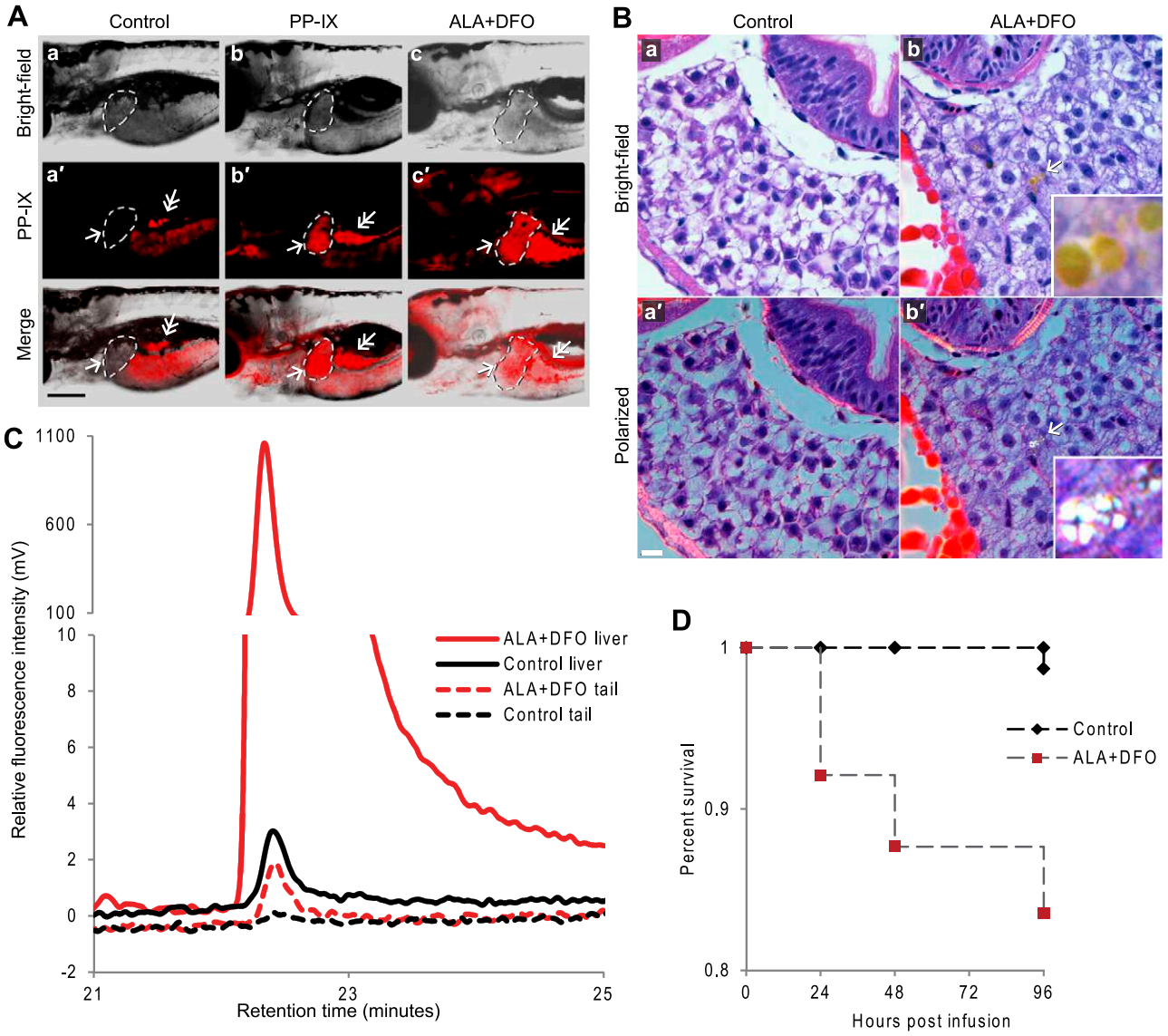

Figure 1. PP-IX accumulates in livers of zebrafish larvae after infusion with PP-IX or ALA + DFO. *A*) Larvae (6 d after fertilization) were infused with DMSO (control) (*a*, *a′*), PP-IX (*b*, *b′*), or ALA + DFO (*c*, *c′*) and imaged by brightfield light (*a–c*) or PP-IX immunofluorescence (*a′–c′*) 5 h after infusion. Larvae infused with PP-IX or ALA + DFO showed strong fluorescence from PP-IX in the liver (single arrows and dashed outline) and intestine (double arrows). Scale bar, 200 μm. At least 10 larvae were observed for each infusion condition. *B*) Larvae were infused with H_2O (control) (*a*, *a′*) or ALA + DFO (*b*, *b′*) and imaged by brightfield (*a*, *b*) or polarized light (*a′*, *b′*). Histologic sections from larvae infused on 2 consecutive days with ALA + DFO contained several pigmented deposits (arrow and inset, *b*) that were birefringent under polarized light. Maltese crosses (arrow and inset, *b′*), characteristic of protoporphyria, were observed. Scale bar, 20 μm. *C*) PP-IX accumulates in the livers of larvae infused with ALA + DFO but not in tail tissue. Control livers and tail tissue from larvae infused with ALA + DFO contained trace levels of PP-IX. *D*) Kaplan-Meier survival curves for control and ALA + DFO–infused larvae. Larvae were shielded from light during the experiment. $P < 0.01$ for 96 h after infusion time point (χ^2 test), n = 73–77/time point per condition.

phenotype than infusion of PP-IX. Another advantage is that both ALA and DFO are carried in a less toxic solvent (H_2O) than PP-IX (DMSO). To determine whether porphyrin was deposited in the liver, cross-sections of larvae infused with ALA + DFO were prepared and analyzed. Few deposits were noted in larvae receiving a single infusion of ALA + DFO, but larvae infused on 2 consecutive days developed several pigmented deposits in the liver. These deposits were birefringent under polarized light, yielding Maltese crosses (Fig. 1*B*) that are characteristic of porphyrin deposits in liver biopsy samples of patients with EPP (2, 39).

Because the heme precursor ALA was used to induce the production of porphyrins, HPLC was used to determine which porphyrins are produced in the zebrafish. Liver and tail tissue (used as an extrahepatic control tissue) of larvae infused with H_2O or ALA + DFO were microdissected, pooled, and homogenized. Analysis by HPLC revealed massive accumulation of PP-IX in the livers of larvae infused with ALA + DFO (Fig. 1*C*). Basal levels of PP-IX were noted in control livers but not tails, and a slight increase in PP-IX was noted in tail tissue of larvae infused with ALA + DFO (Fig. 1*C*), perhaps as a result of circulating porphyrins or limited accumulation in cutaneous tissue. Similar to

patients with EPP, PP-IX was the predominant porphyrin that accumulated in the liver, although slightly increased levels of uroporphyrin and coproporphyrin were also detected (data not shown). Lethality was assessed in larvae for the first 96 h after infusion with H_2O or ALA + DFO. Significantly higher mortality was observed (~15%) in larvae infused with ALA + DFO *versus* control larvae infused with H_2O (Fig. 1*D*).

Porphyrin accumulation peaks at 24 h followed by excretion into fish water

To determine the time course of porphyrin accumulation, zebrafish larvae that express eGFP-tagged fibrinogen β were imaged at 5, 24, 72, and 144 h after ALA + DFO infusion or at 24 and 144 h after infusion with H_2O. Larvae were microdissected and the porphyrin levels quantified in liver and tail tissues at each time point. Significant porphyrin fluorescence was observed 5 h after infusion but was highest 24 h after infusion (**Fig. 2*A***). Fluorescence was virtually undetectable at 72 and 144 h after infusion (Fig. 2*A*), thereby suggesting that the porphyrins were excreted or metabolized to heme, which is not fluorescent. Control larvae infused with H_2O did not show significant fluorescence at any time point assessed (Fig. 1*Aa″*, *b″*). Close inspection of livers from larvae at 72 h after infusion revealed a significant number of pigmented deposits (data not shown), presumed to be PP-IX crystals. Homogenized livers from larvae infused with ALA + DFO contained a significant amount of PP-IX 5 h after infusion (275 pmol/mg protein) that peaked from 24 to 72 h (3815–4000 pmol/mg protein, respectively) (Fig. 2*B*). Porphyrin levels then fell to half of peak levels (1781 pmol/mg protein) at 144 h after infusion (Fig. 2*B*). The gallbladders of larvae infused with ALA + DFO often contained large pigmented crystalline deposits (Fig. 2*C*), similar to those reported in patients with EPP (2, 40), suggesting that the porphyrins are cleared through the biliary system. To determine which porphyrins were being excreted, the fish water of infused larvae was collected and analyzed by HPLC. As expected, PP-IX was the primary excreted porphyrin (Fig. 2*D*), but limited levels of coproporphyrin were also detected (data not shown). It is noteworthy that increased levels of urinary coproporphyrin have been noted in cases of liver damage in patients with EPP (11). The highest level of porphyrin excretion was after the first 24 h after infusion, but it continued through 96 h after infusion (Fig. 2*D*).

ALA + DFO–mediated porphyrin accumulation is inhibited by coinfusion of SA

Previous studies have shown that administering metal chelators, such as EDTA and DFO, may increase the production of PP-IX (41, 42) because metalloporphyrins may negatively regulate the heme biosynthetic pathway through feedback inhibition (43). Infusion of H_2O or DFO alone does not cause significant porphyrin fluorescence in the liver of zebrafish larvae; however, infusion of ALA alone results in noticeable porphyrin fluorescence (**Fig. 3**). This liver fluorescence increases dramatically when DFO is coinfused with ALA and more porphyrin deposits become visible (Fig. 3*Ad*). Coinfusing SA, which prevents utilization of ALA for the production of porphyrins by inhibiting ALA dehydratase activity (44), with ALA + DFO results in decreased liver fluorescence intensity in the infused larvae (Fig. 3*Ac″–e″*; *B*). These results further support the specificity of the phenotype we observed and are similar to heme biosynthesis regulation that has been reported in humans and murine models (41–44).

Porphyrin accumulation causes hepatic protein aggregation and ultrastructural alterations

Previous reports demonstrated that nuclear lamins are a sensitive marker for porphyrin-induced protein aggregation in mice with genetic (*FECH* mutation) or DDC-induced porphyria (15). We tested the hypothesis that lamins would aggregate in the livers of larvae infused with ALA + DFO but not in tail tissues as a result of the tissue-specific accumulation of PP-IX in the liver. Livers and tails were pooled from larvae that had been infused with H_2O or ALA + DFO, followed by immunoblotting with anti-lamin B1 antibody. Larvae infused with ALA + DFO showed prominent high-molecular-weight lamin B1 reactivity in liver tissue compared to controls (**Fig. 4*A***). No significant differences were noted in protein aggregation of tail tissue homogenates.

We then asked whether additional aggregated proteins could be detected by MS analysis of liver tissue protein isolates. Notably, proteins from various subcellular compartments in the liver aggregated upon ALA + DFO administration (Fig. 4*B*, Supplemental Table S1). Several of the strongest readouts were of proteins known to be located in the ER. We validated the aggregation of the ER protein PDI (Fig. 4*C*), which was detected by MS analysis.

Given the biochemical evidence for multiorganelle protein aggregation, we used transmission electron microscopy and ultrastructural analysis to test whether ALA + DFO treatment caused alterations that might be similar to what is observed in human porphyria. As shown in **Fig. 5**, nuclear membrane ruffling, electron-dense deposits, and autophagosomes were prominent in livers of ALA + DFO–infused larvae. Hepatocytes with dilated rough ER were also noted (data not shown). These ultrastructural alterations support a porphyria-mediated proteotoxic effect, probably because of protein aggregation.

Porphyria-associated protein misfolding causes ER stress and activation of autophagy

The ER proteins PERK, ATF6, and IRE1 are capable of sensing aggregated or misfolded proteins in the context of ER stress (45). IRE1 and ATF6 may then splice *XBP1* mRNA and induce its transcription, respectively (46). Spliced *XBP1* is necessary for activating the UPR (46). As soon as 4 h after infusion of larvae with ALA + DFO, we noted increased levels of spliced *xbp1* mRNA (*xbp1s*), *chop,* and *atf3* transcripts (**Fig. 6*A***). These transcripts represent early-phase responses and are regulated by different signaling pathways

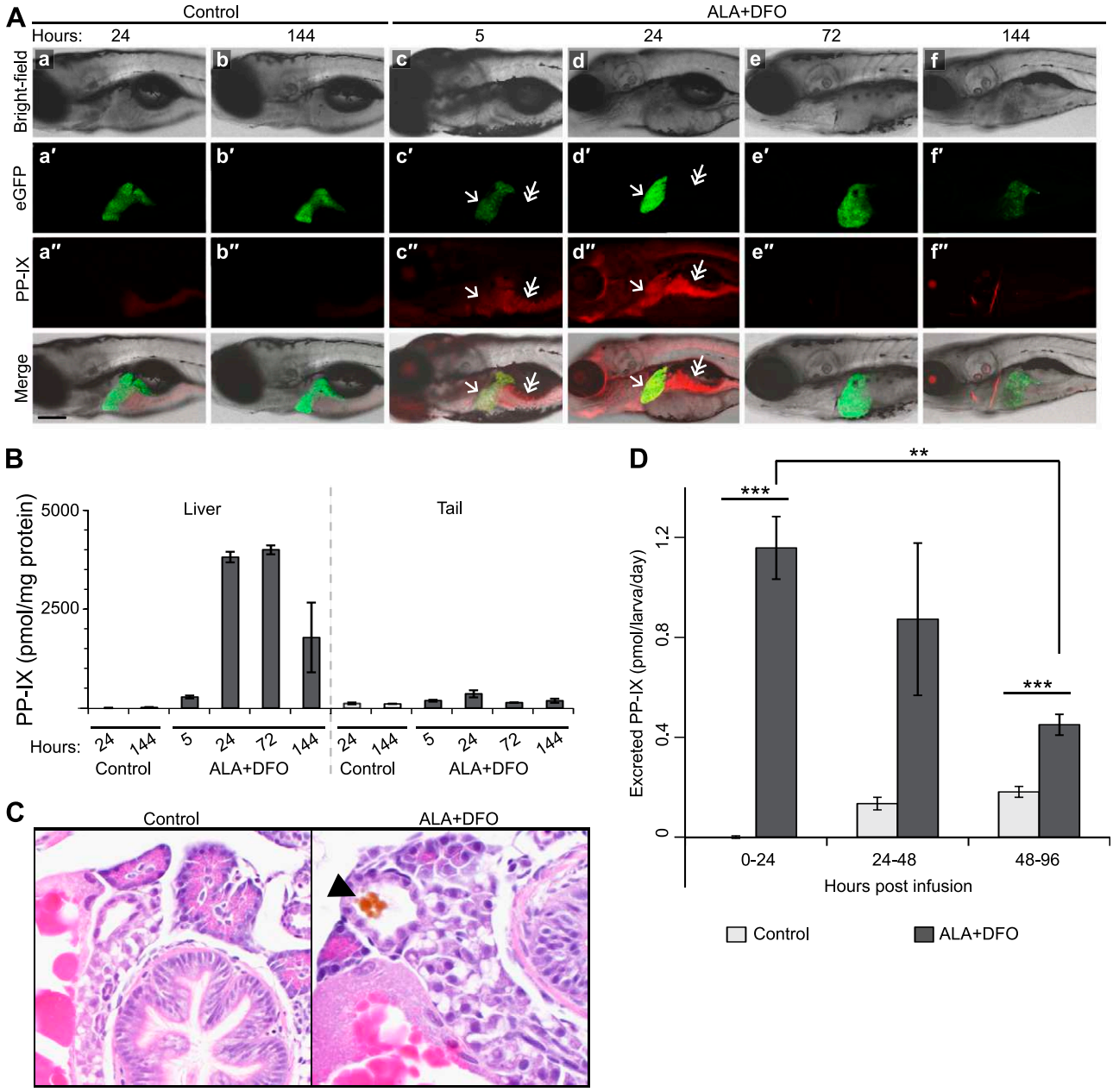

Figure 2. Time-dependent porphyrin accumulation and excretion. *A*) Larvae were infused with H_2O (control) (*a*–*b*″) or ALA + DFO (*c*–*f*″) and imaged by brightfield light (*a*–*f*) or eGFP (*a*′–*f*′) or PP-IX immunofluorescence (*a*″–*f*″) for 5 h (*c*–*c*″), 24 h (*a*–*a*″, *d*–*d*″), 72 h (*e*–*e*″), or 144 h (*b*–*b*″, *f*–*f*″). Larvae infused with ALA + DFO showed significant fluorescence by 5 h and peaked at 24 h, with PP-IX concentrating in liver (arrows) and intestine (double arrows). Fluorescence was virtually undetectable at 72 and 144 h after infusion. No significant changes in liver size were noted. Scale bar, 200 μm. At least 10 larvae were observed for each time point. *B*) Liver and tail tissue of larvae infused with H_2O or ALA + DFO was dissected, homogenized, and porphyrin content was quantified. PP-IX was nearly undetectable in the livers of control larvae, but livers of larvae infused with ALA + DFO accumulated PP-IX as soon as 5 h after infusion. Porphyrin content was highest at 24 and 72 h after infusion, and fell 144 h after infusion. No significant changes in porphyrin content of tail tissues between control and ALA + DFO–infused larvae were observed (n = 3 groups). *C*) Porphyrin deposits (arrowhead) were noted in the gallbladder of hematoxylin and eosin–stained cross sections of larvae infused with ALA + DFO, but not in control larvae. *D*) PP-IX was detected in fish water of larvae infused with ALA + DFO. Excretion was undetectable 15 min after infusion (not shown) and peaked during the first 24 h after infusion. Excretion decreased 48–96 h after infusion but was still greater than control larvae. n = 3 wells per time point. $^{**}P < 0.01$, $^{***}P < 0.001$ (2-tailed Student's t test); error bars indicate SE.

(46–48). The increased transcription of *atf3* at 4 and 12 h after infusion was not observed 24 h after infusion, further suggesting that it plays a role in the early-phase stress response. Increased expression of *chop* was observed at 4 and 12 h after infusion (Fig. 6*A*), as might be expected based on previous reports of CHOP induction by ATF3 (48). Increased expression of *atf6* (Fig. 6*A*) was only observed 24 h after infusion, perhaps indicating an additional role in the late-phase response to ER stress. Cleavage of the ATF6 protein in the early-phase response has been well characterized as an upstream indicator and plays an important role in the activation of the UPR (36, 49, 50).

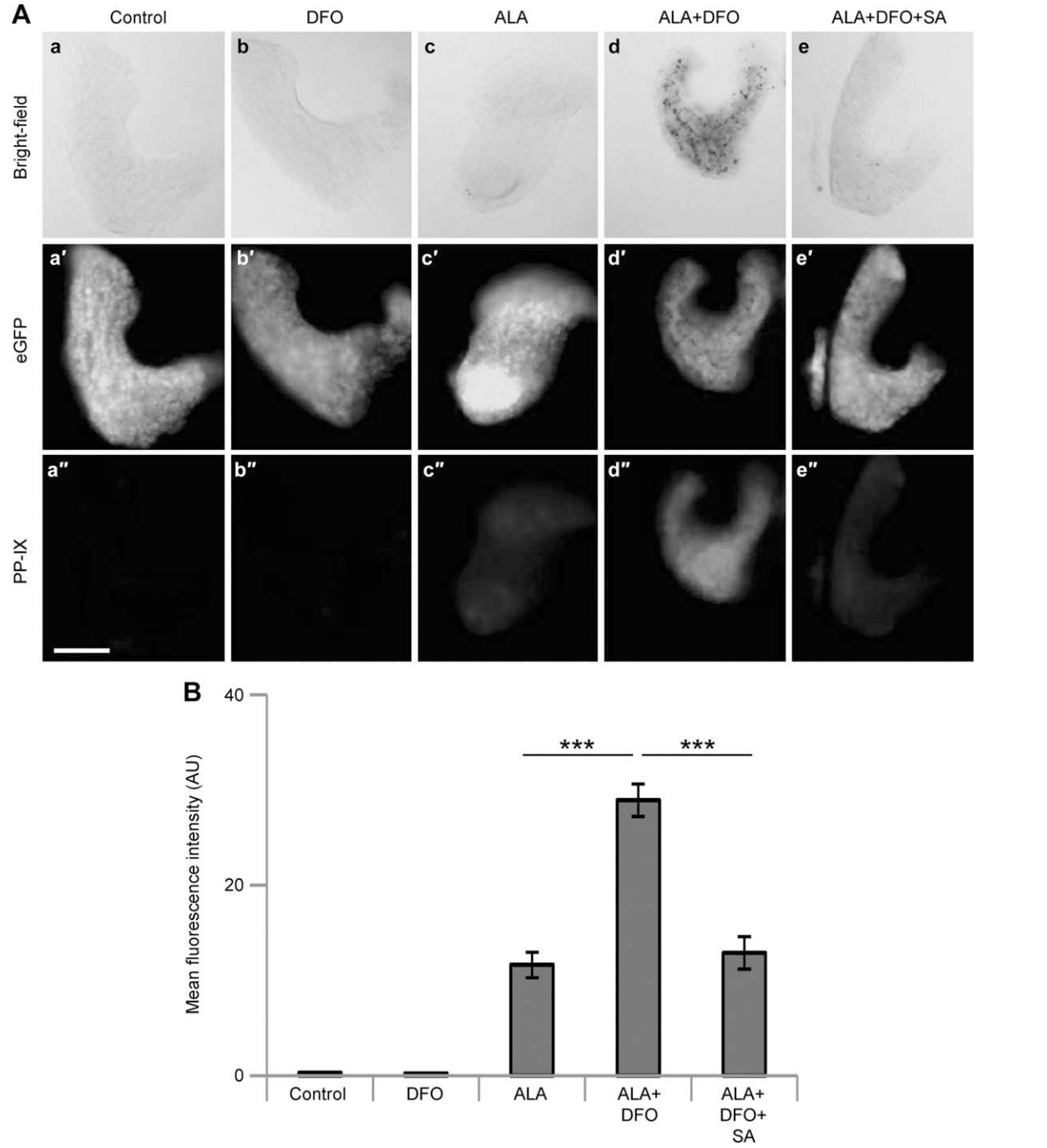

Figure 3. Specificity of porphyrin liver accumulation in response to ALA + DFO infusion. *A*) Five days after fertilization, larvae were infused with H_2O (*a*–*a*″), DFO (*b*–*b*″), ALA (*c*–*c*″), ALA + DFO (*d*–*d*″), or ALA + DFO + SA (*e*–*e*″). Livers were visualized under green fluorescence to assist in their identification, microdissected, and subsequently imaged using brightfield light (*a*–*e*), eGFP (to detect the fluorescent livers) (*a*′–*e*′) and Texas Red (to detect PP-IX fluorescence) (*a*″–*e*″) filters. Larvae infused with ALA (*c*″), ALA + DFO (*d*″), or ALA + DFO + SA (*e*″) had significant liver PP-IX fluorescence, although the greatest fluorescence intensity was noted in livers of larvae infused with ALA + DFO (*d*″). Livers of larvae infused with ALA + DFO also contained dark crystalline deposits that are readily visualized in (*d*). Scale bar, 100 μm. *B*) Quantification of PP-IX fluorescence using ImageJ software; $n = 9$–21 livers per group; error bars represent SE. Statistical analysis was performed by 2-tailed Student's *t* test, $^{***}P < 0.001$.

One possible mechanism to reduce the number of misfolded or aggregated proteins is through degradation by autophagy. Increased expression of *atg5* and *atg16l1* were noted 24 h after infusion (Fig. 6*A*), consistent with the upstream role of ER stress and the UPR in activating autophagy. These genes code for proteins involved in autophagosome formation and are induced by the transcription factors chop and atf4, respectively (51, 52). Transcription of *becn1,* a gene that codes for beclin1, a protein involved in the formation of the autophagosome, was not significantly altered between the control and ALA + DFO groups at any of the time points measured (Fig. 6*A*).

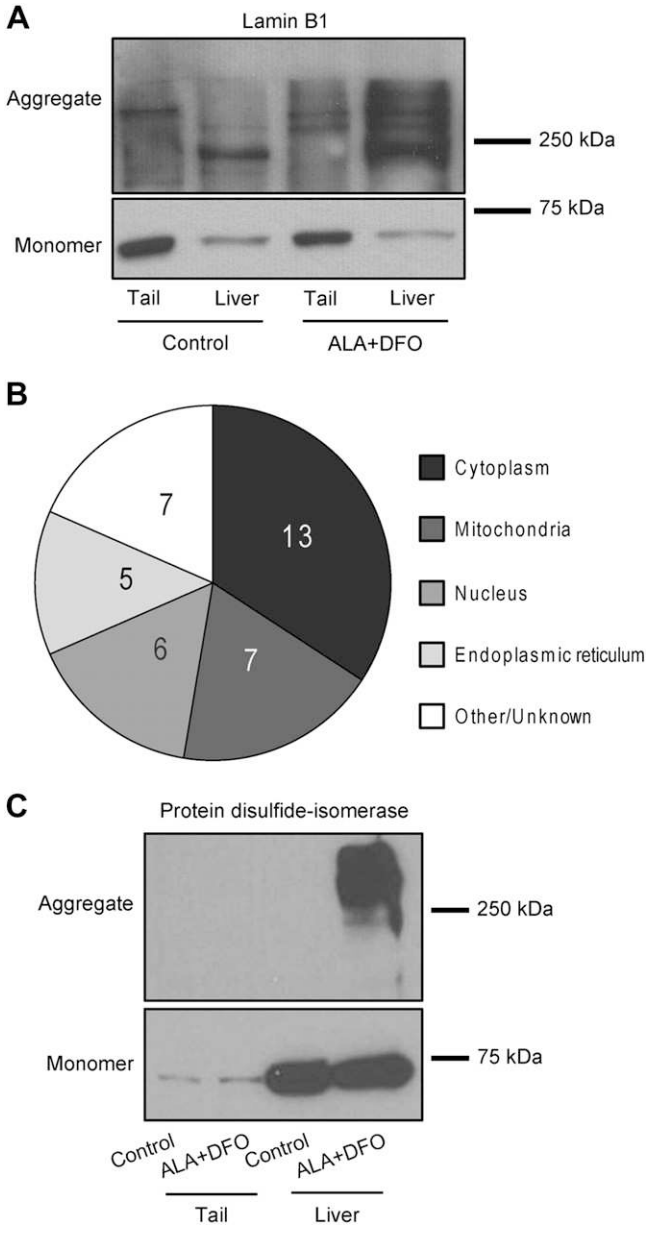

Figure 4. Porphyrin accumulation causes multiorganelle protein aggregation. *A*) Liver tissue, but not tail tissue, of larvae infused with ALA + DFO contained high-molecular-weight aggregates of lamin B1 as determined by immunoblotting. *B*) MS identified 38 proteins that were aggregated in livers of larvae infused with ALA + DFO but not with H_2O. Most proteins were in the cellular compartments of cytoplasm, mitochondria, nucleus, and ER (Supplemental Table S1). Most highly aggregated proteins tended to reside in ER (with identification using UniProt data set; http://www.uniprot.org). *C*) Immunoblotting with specific rabbit antibody to PDI was used to confirm the MS results. Only livers of larvae infused with ALA + DFO showed significant high-molecular-weight species reactivity.

We used the LysoTracker dye, which has been used in zebrafish, to detect changes in autophagic flux by accumulating in acidic compartments such as autophagosomes (53). Larvae were stained with the LysoTracker dye 24 h after infusion of ALA + DFO. The stained livers had significantly greater numbers of positive puncta than controls (Fig. 6*B*), thereby supporting the induction of autophagy. There was no direct colocalization between positive lysosomal puncta and porphyrin deposits. These findings are consistent with the autophagosomes we observed by transmission electron microscopy (Fig. 5*D*), which are similar to what has been previously described in mammalian systems (54).

The ER stress and autophagy-induction findings in zebrafish were validated in 2 mouse models of porphyria: the FECH knockout model and a subacute porphyria model that involves 5 d of DDC feeding. In both models, porphyrin accumulation (Fig. 6*C*) was associated with increased nuclear CHOP and ATF4, as well as increased LC3B-II levels (relative to LC3B-I) (Fig. 6*D*).

DISCUSSION

We present 2 new acute zebrafish models of protoporphyria that phenocopy many of the characteristics of protoporphyria in patients. These characteristics include light sensitivity, accumulation of PP-IX in the liver with the characteristic Maltese cross, excretion of PP-IX and coproporphyrin through the biliary system, protein aggregation, and ultrastructural alterations. In addition, we describe the induction of the UPR and autophagy in zebrafish and mouse models of protoporphyria. The zebrafish models described herein, particularly the ALA + DFO model, provide distinct advantages that complement the previously described genetic zebrafish porphyria models (30–32). In practical terms, the model is relatively simple given that it is induced by a single retroorbital infusion of the heme precursor ALA, the iron chelator DFO, or the infusion of PP-IX alone. This model system allows for flexibility in terms of designing experiments and performing chemical and genetic screens. In our hands, at least 250 larvae may be infused per hour, thereby making it a high-throughput model system. Genetic (55) and inducible murine models (56, 57) of porphyrias exist, but zebrafish larvae enable large-scale chemical and genetic screens. The ease of imaging, high fecundity, and rapid and external development and relatively low financial cost are known benefits for zebrafish models (58, 59), which make zebrafish a particularly useful model organism.

We describe 2 protoporphyria zebrafish models: XLP through infusion of ALA + DFO and EPP by infusion of PP-IX (**Fig. 7*A***). The XLP model is more robust and less variable than the PP-IX infusion model; we speculate that this may be due to the relative insolubility of PP-IX once it is introduced systemically. A similar approach may be taken to produce other porphyrias by infusing different heme precursors or compounds that inhibit enzymes in the heme biosynthesis pathway. As an example, a zebrafish model for ALA-dehydratase deficiency porphyria could be produced by infusing ALA with SA, a small molecule that blocks the catalytic activity of ALA-dehydratase (44). This would be expected to result in high circulating levels of ALA, as described in patients with ALA-dehydratase deficiency porphyria (60). This flexibility, combined with the fluorescent nature of porphyrins, renders inducible zebrafish porphyria models ideal systems to identify porphyrin transport proteins and characterize additional

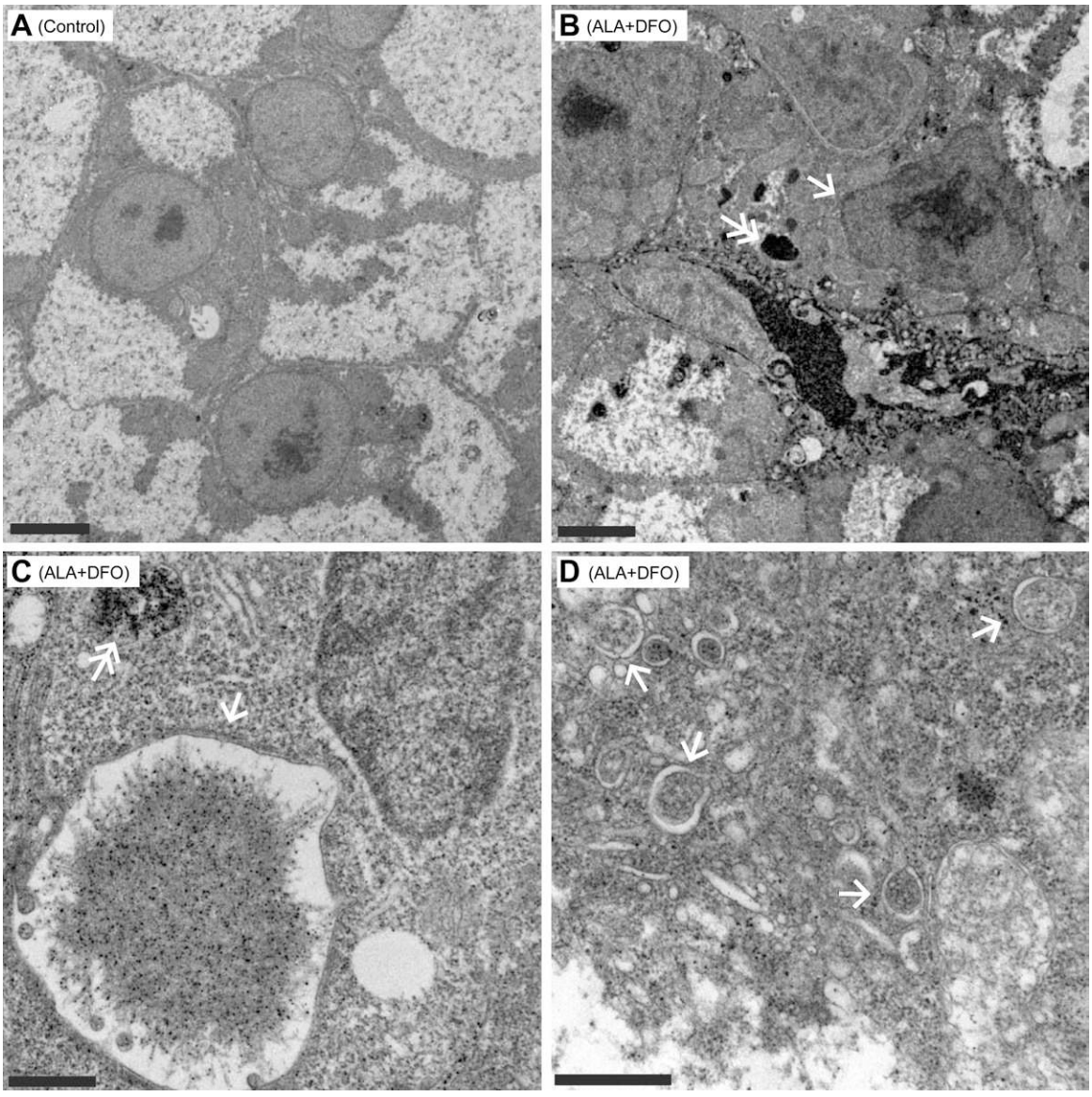

Figure 5. Ultrastructural analysis of livers from larvae infused with H_2O or ALA + DFO. Transmission electron micrographs were prepared from livers of zebrafish infused on 2 consecutive days with H_2O or ALA + DFO. *A*) Control hepatocytes show distinct rough ER with no ultrastructural abnormalities; scale bar, 3 μm. *B*) Hepatocytes from larvae infused with ALA + DFO showed high proportion of distorted nuclei (82% for ALA + DFO infused *vs.* 30% for H_2O infused, $P < 0.001$, 2-proportion *z* test) (arrow) and high levels of electron-dense amorphous material (28% *vs.* 2% $P < 0.001$, 2-proportion *z* test) (double arrow). Scale bar, 3 μm, $n = 87–107$ cells from 3 different larvae per condition. *C*) High magnification revealed the electron-dense material was membrane bound (double arrow). Some cells contained large membrane-bound amorphous material (arrow); scale bar, 0.6 μm. *D*) Numerous autophagosomes (arrows) were observed in hepatocytes of larvae infused with ALA + DFO; this was not observed in control hepatocytes; scale bar, 0.6 μm.

genetic and molecular aspects of porphyrias. One potential limitation of our model is that it does not lead to chronic disease because the PP-IX is efficiently cleared (Fig. 2*D*).

Porphyrins are known to cause oxidative stress in the absence of light (21, 22, 24, 61), but concomitant porphyrin-mediated protein aggregation in mice and cell culture systems has not been reported until recently (15, 35). The effects of protein aggregation are not well known in the context of porphyria-induced tissue damage. Previous reports have described porphyrin-associated ultrastructural changes in the ER, mitochondria, and nucleus in mammalian systems (21, 62), consistent with our findings of cytoplasmic and multiorganelle protein aggregation in the livers of the zebrafish larvae (Fig. 7*B*). The ultrastructural alterations we observed are supported by our detection of aggregated lamins, PDI, and other proteins. Misfolded or aggregated proteins may cause ER stress, which is associated with numerous diseases (28, 29), but their pathophysiologic role in porphyria has not been established. Ultrastructural analysis of liver samples from patients with EPP has revealed dilated rough ER (63), consistent with ER stress, although the potential presence of protein aggregates in patient sample groups has not

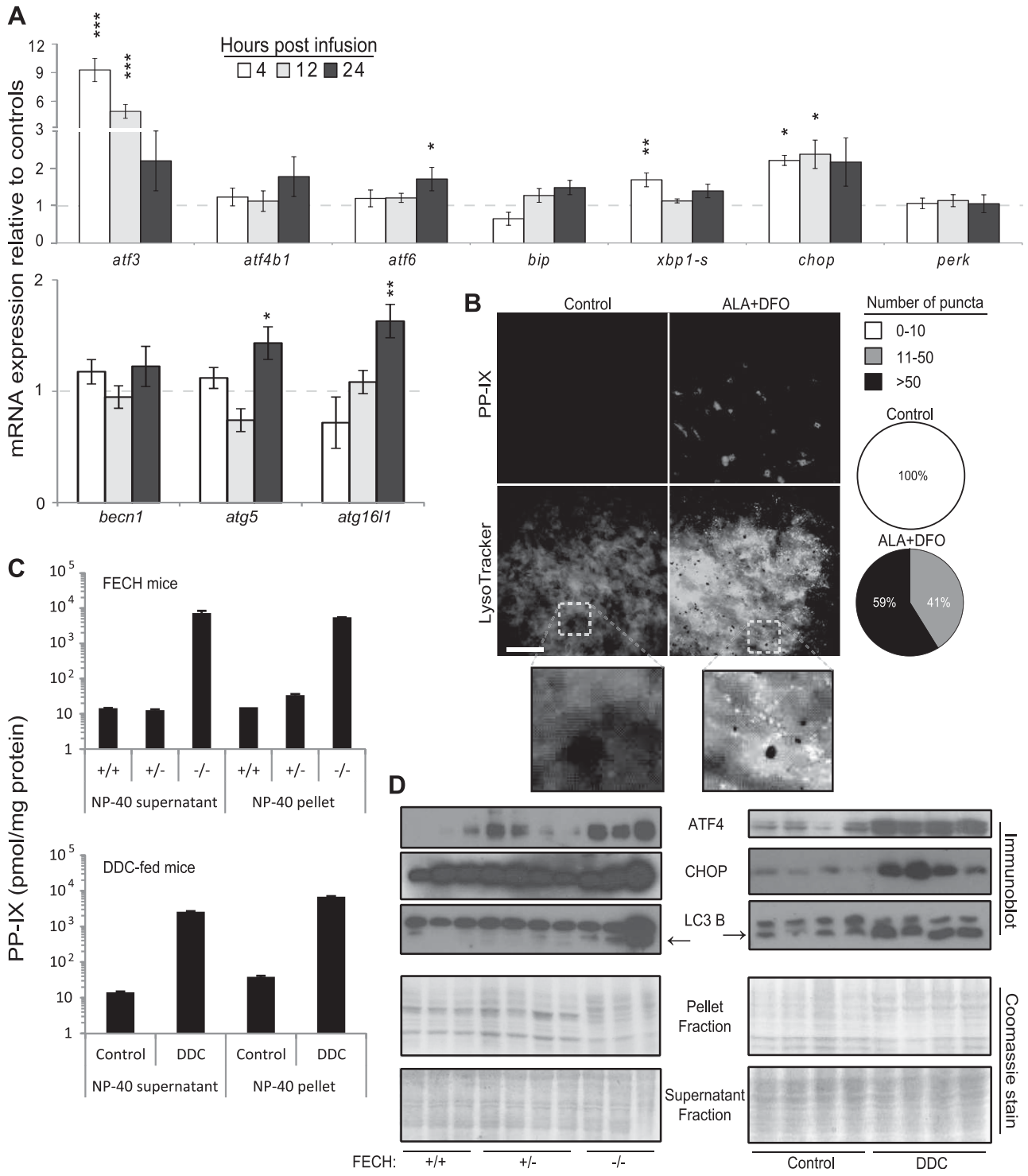

Figure 6. Hepatic ER stress and induction of autophagy in association with porphyrin accumulation. *A*) ER stress-associated transcripts were up-regulated in livers of larvae infused with ALA + DFO. Error bars represent SE. $*P < 0.05$, $**P < 0.01$, $***P < 0.001$ (2-tailed Student's *t* test). Transcripts *atg5* and *atg16l1* were up-regulated only 24 h after infusion with ALA + DFO, thereby suggesting autophagy induction. All transcripts were compared to those isolated from larvae infused with H_2O and collected at 5, 12, or 24 h after infusion. $*P < 0.05$, $**P < 0.01$. *B*) LysoTracker dye was used to stain acidic cellular compartments of livers from larvae infused with H_2O or ALA + DFO. Puncta per liver were counted and placed into 3 categories (based on number of puncta): 0–10 (low), 11–50 (medium), or >50 (high). A χ^2 test was used to determine significance ($P < 0.001$). Magnification of the dotted areas is shown in corresponding lower panels. Scale bar = 50 μm. *C*) Porphyrin accumulates in livers of mice containing biallelic *FECH* mutation and in mice fed DDC. *D*) LC3B-II (lower band highlighted by arrows) and nuclear ATF4 and CHOP are up-regulated in livers of *FECH* $^{-/-}$ mice and mice fed DDC.

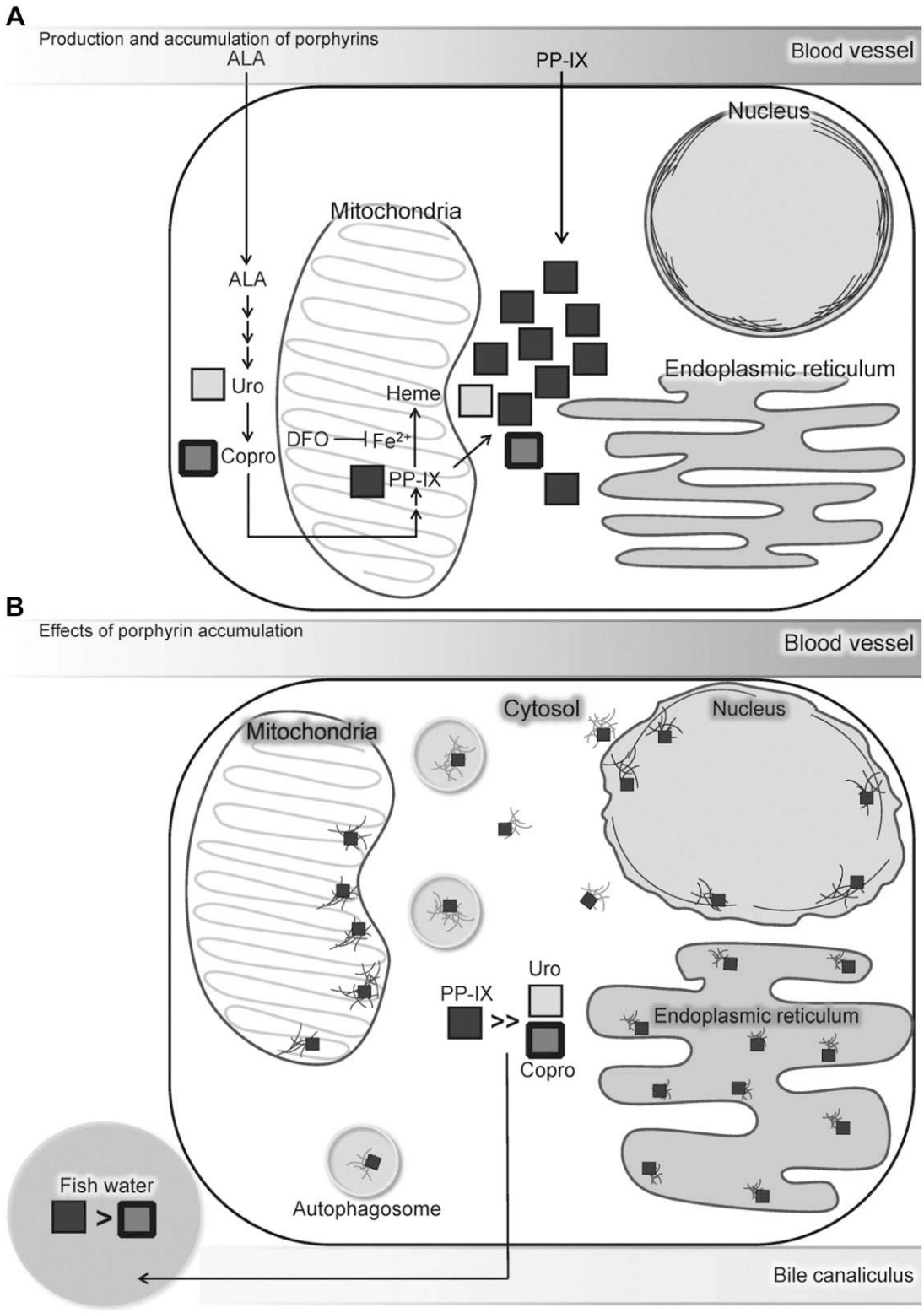

Figure 7. Models of porphyrin accumulation and cellular response. *A*) Infused ALA is metabolized to uroporphyrin and coproporphyrin but mainly results in PP-IX accumulation. DFO chelates free iron to prevent synthesis of heme. Alternatively, PP-IX may be infused directly. *B*) Porphyrin accumulation in liver causes multiorganelle and compartment protein aggregation in cytoplasm, mitochondria, nucleus, and ER. Swollen ER depicts induction of ER stress. Circles represent autophagosomes, which may play a role in clearing protein aggregates to relieve ER stress. PP-IX (in much larger amounts) and coproporphyrin are excreted into fish water through biliary system.

been tested. Future studies will be directed toward defining the mechanism of aggregate clearance. FJ

This work was supported in part by the U.S. National Institutes of Health (NIH) National Institute of Diabetes and Digestive and Kidney Diseases (NIDDK) Grant R01-DK52951 and the Department of Veterans Affairs (M.B.O.); NIH National Heart, Lung, and Blood Institute Grant R01-HL124232 (J.A.S.); and NIH NIDDK Institutional Grants DK034933 and DK020572 to the University of Michigan. The authors thank S. E. Whitesall and L. G. D'Alecy for assistance with the HPLC analysis, the University of Michigan Unit for Laboratory Animal Medicine In Vivo Animal Core for their assistance with obtaining histological sections of zebrafish larvae, and V. Basrur for carrying out the MS analysis with support from the University of Michigan Protein Folding Diseases Initiative. The authors declare no conflicts of interest.

REFERENCES

1. Gross, U., Hoffmann, G. F., and Doss, M. O. (2000) Erythropoietic and hepatic porphyrias. *J. Inherit. Metab. Dis.* **23**, 641–661
2. Lecha, M., Puy, H., and Deybach, J.-C. (2009) Erythropoietic protoporphyria. *Orphanet J. Rare Dis.* **4**, 19
3. Balwani, M., and Desnick, R. J. (2012) The porphyrias: advances in diagnosis and treatment. *Blood* **120**, 4496–4504
4. Bonkovsky, H. L., Guo, J. T., Hou, W., Li, T., Narang, T., and Thapar, M. (2013) Porphyrin and heme metabolism and the porphyrias. *Compr. Physiol.* **3**, 365–401
5. Taketani, S., Nakahashi, Y., Osumi, T., and Tokunaga, R. (1990) Molecular cloning, sequencing, and expression of mouse ferrochelatase. *J. Biol. Chem.* **265**, 19377–19380
6. Bottomley, S. S., Tanaka, M., and Everett, M. A. (1975) Diminished erythroid ferrochelatase activity in protoporphyria. *J. Lab. Clin. Med.* **86**, 126–131
7. Nakahashi, Y., Fujita, H., Taketani, S., Ishida, N., Kappas, A., and Sassa, S. (1992) The molecular defect of ferrochelatase in a patient with erythropoietic protoporphyria. *Proc. Natl. Acad. Sci. USA* **89**, 281–285
8. Elder, G. H., Gouya, L., Whatley, S. D., Puy, H., Badminton, M. N., and Deybach, J. C. (2009) The molecular genetics of erythropoietic protoporphyria. *Cell. Mol. Biol. (Noisy-le-grand)* **55**, 118–126
9. Whatley, S. D., Ducamp, S., Gouya, L., Grandchamp, B., Beaumont, C., Badminton, M. N., Elder, G. H., Holme, S. A., Anstey, A. V., Parker, M., Corrigall, A. V., Meissner, P. N., Hift, R. J., Marsden, J. T., Ma, Y., Mieli-Vergani, G., Deybach, J. C., and Puy, H. (2008) C-terminal deletions in the *ALAS2* gene lead to gain of function and cause X-linked dominant protoporphyria without anemia or iron overload. *Am. J. Hum. Genet.* **83**, 408–414
10. Shemin, D. (1970) On the synthesis of heme. *Naturwissenschaften* **57**, 185–190
11. Gross, U., Frank, M., and Doss, M. O. (1998) Hepatic complications of erythropoietic protoporphyria. *Photodermatol. Photoimmunol. Photomed.* **14**, 52–57
12. Meerman, L. (2000) Erythropoietic protoporphyria. An overview with emphasis on the liver. *Scand. J. Gastroenterol. Suppl.* **(232)**, 79–85
13. Sarkany, R. P., Alexander, G. J., and Cox, T. M. (1994) Recessive inheritance of erythropoietic protoporphyria with liver failure. *Lancet* **343**, 1394–1396
14. Whatley, S. D., Mason, N. G., Khan, M., Zamiri, M., Badminton, M. N., Missaoui, W. N., Dailey, T. A., Dailey, H. A., Douglas, W. S., Wainwright, N. J., and Elder, G. H. (2004) Autosomal recessive erythropoietic protoporphyria in the United Kingdom: prevalence and relationship to liver disease. *J. Med. Genet.* **41**, e105
15. Singla, A., Griggs, N. W., Kwan, R., Snider, N. T., Maitra, D., Ernst, S. A., Herrmann, H., and Omary, M. B. (2013) Lamin aggregation is an early sensor of porphyria-induced liver injury. *J. Cell Sci.* **126**, 3105–3112
16. Omary, M. B., Coulombe, P. A., and McLean, W. H. I. (2004) Intermediate filament proteins and their associated diseases. *N. Engl. J. Med.* **351**, 2087–2100
17. Aguzzi, A., and O'Connor, T. (2010) Protein aggregation diseases: pathogenicity and therapeutic perspectives. *Nat. Rev. Drug Discov.* **9**, 237–248
18. Zatloukal, K., Stumptner, C., Fuchsbichler, A., Heid, H., Schnoelzer, M., Kenner, L., Kleinert, R., Prinz, M., Aguzzi, A., and Denk, H. (2002) p62 is a common component of cytoplasmic inclusions in protein aggregation diseases. *Am. J. Pathol.* **160**, 255–263
19. Kwan, R., Hanada, S., Harada, M., Strnad, P., Li, D. H., and Omary, M. B. (2012) Keratin 8 phosphorylation regulates its transamidation and hepatocyte Mallory-Denk body formation. *FASEB J.* **26**, 2318–2326
20. Tsunoo, C., Harwood, T. R., Arak, S., and Yokoo, H. (1987) Cytoskeletal alterations leading to Mallory body formation in livers of mice fed 3,5-diethoxycarbonyl-1,4-dihydrocollidine. *J. Hepatol.* **5**, 85–97
21. Koningsberger, J. C., Rademakers, L. H. P. M., van Hattum, J., de la Faille, H. B., Wiegman, L. J. J. M., Italiaander, E., van Berge Henegouwen, G. P., and Marx, J. J. M. (1995) Exogenous protoporphyrin inhibits Hep G2 cell proliferation, increases the intracellular hydrogen peroxide concentration and causes ultrastructural alterations. *J. Hepatol.* **22**, 57–65
22. Afonso, S., Vanore, G., and Batlle, A. (1999) Protoporphyrin IX and oxidative stress. *Free Radic. Res.* **31**, 161–170
23. Singla, A., Moons, D. S., Snider, N. T., Wagenmaker, E. R., Jayasundera, V. B., and Omary, M. B. (2012) Oxidative stress, Nrf2 and keratin up-regulation associate with Mallory-Denk body formation in mouse erythropoietic protoporphyria. *Hepatology* **56**, 322–331
24. Morehouse, K. M., Moreno, S. N., and Mason, R. P. (1987) The one-electron reduction of uroporphyrin I by rat hepatic microsomes. *Arch. Biochem. Biophys.* **257**, 276–284
25. Morehouse, K. M., and Mason, R. P. (1990) The enzymatic one-electron reduction of porphyrins to their anion free radicals. *Arch. Biochem. Biophys.* **283**, 306–310
26. Ron, D., and Walter, P. (2007) Signal integration in the endoplasmic reticulum unfolded protein response. *Nat. Rev. Mol. Cell Biol.* **8**, 519–529
27. Cao, S. S., and Kaufman, R. J. (2012) Unfolded protein response. *Curr. Biol.* **22**, R622–R626
28. Marciniak, S. J., and Ron, D. (2006) Endoplasmic reticulum stress signaling in disease. *Physiol. Rev.* **86**, 1133–1149
29. Zhao, L., and Ackerman, S. L. (2006) Endoplasmic reticulum stress in health and disease. *Curr. Opin. Cell Biol.* **18**, 444–452
30. Childs, S., Weinstein, B. M., Mohideen, M.-A. P. K., Donohue, S., Bonkovsky, H., and Fishman, M. C. (2000) Zebrafish dracula encodes ferrochelatase and its mutation provides a model for erythropoietic protoporphyria. *Curr. Biol.* **10**, 1001–1004
31. Dooley, K. A., Fraenkel, P. G., Langer, N. B., Schmid, B., Davidson, A. J., Weber, G., Chiang, K., Foott, H., Dwyer, C., Wingert, R. A., Zhou, Y., Paw, B. H., and Zon, L. I.; Tübingen 2000 Screen Consortium. (2008) Montalcino, a zebrafish model for variegate porphyria. *Exp. Hematol.* **36**, 1132–1142
32. Wang, H., Long, Q., Marty, S. D., Sassa, S., and Lin, S. (1998) A zebrafish model for hepatoerythropoietic porphyria. *Nat. Genet.* **20**, 239–243
33. Lieschke, G. J., and Currie, P. D. (2007) Animal models of human disease: zebrafish swim into view. *Nat. Rev. Genet.* **8**, 353–367
34. Vo, A. H., Swaroop, A., Liu, Y., Norris, Z. G., and Shavit, J. A. (2013) Loss of fibrinogen in zebrafish results in symptoms consistent with human hypofibrinogenemia. *PLoS One* **8**, e74682
35. Maitra, D., Elenbaas, J. S., Whitesall, S. E., Basrur, V., D'Alecy, L. G., and Omary, M. B. (2015) Ambient light promotes selective subcellular proteotoxicity after endogenous and exogenous porphyrinogenic stress. *J. Biol. Chem.* **290**, 23711–23724
36. Cinaroglu, A., Gao, C., Imrie, D., and Sadler, K. C. (2011) Activating transcription factor 6 plays protective and pathological roles in steatosis due to endoplasmic reticulum stress in zebrafish. *Hepatology* **54**, 495–508
37. Goldsmith, J. R., Cocchiaro, J. L., Rawls, J. F., and Jobin, C. (2013) Glafenine-induced intestinal injury in zebrafish is ameliorated by μ-opioid signaling *via* enhancement of Atf6-dependent cellular stress responses. *Dis. Model. Mech.* **6**, 146–159
38. Liu, Y., Kretz, C. A., Maeder, M. L., Richter, C. E., Tsao, P., Vo, A. H., Huarng, M. C., Rode, T., Hu, Z., Mehra, R., Olson, S. T., Joung, J. K., and Shavit, J. A. (2014) Targeted mutagenesis of zebrafish antithrombin III triggers disseminated intravascular coagulation and thrombosis, revealing insight into function. *Blood* **124**, 142–150
39. Thompson, R. P. H., Molland, E. A., Nicholson, D. C., and Gray, C. H. (1973) "Erythropoietic" protoporphyria and cirrhosis in sisters. *Gut* **14**, 934–938

40. Todd, D. J. (1991) Gallstones in children. *Am. J. Dis. Child.* **145**, 971–972
41. Curnow, A., and Pye, A. (2007) Biochemical manipulation *via* iron chelation to enhance porphyrin production from porphyrin precursors. *J. Environ. Pathol. Toxicol. Oncol.* **26**, 89–103
42. Valdés, P. A., Samkoe, K., O'Hara, J. A., Roberts, D. W., Paulsen, K. D., and Pogue, B. W. (2010) Deferoxamine iron chelation increases δ-aminolevulinic acid induced protoporphyrin IX in xenograft glioma model. *Photochem. Photobiol.* **86**, 471–475
43. Sassa, S., and Nagai, T. (1996) The role of heme in gene expression. *Int. J. Hematol.* **63**, 167–178
44. Sassa, S., and Kappas, A. (1983) Hereditary tyrosinemia and the heme biosynthetic pathway. Profound inhibition of delta-aminolevulinic acid dehydratase activity by succinylacetone. *J. Clin. Invest.* **71**, 625–634
45. Rutkowski, D. T., and Kaufman, R. J. (2004) A trip to the ER: coping with stress. *Trends Cell Biol.* **14**, 20–28
46. Yoshida, H., Matsui, T., Yamamoto, A., Okada, T., and Mori, K. (2001) XBP1 mRNA is induced by ATF6 and spliced by IRE1 in response to ER stress to produce a highly active transcription factor. *Cell* **107**, 881–891
47. Chen, B. P., Wolfgang, C. D., and Hai, T. (1996) Analysis of ATF3, a transcription factor induced by physiological stresses and modulated by gadd153/Chop10. *Mol. Cell. Biol.* **16**, 1157–1168
48. Jiang, H.-Y., Wek, S. A., McGrath, B. C., Lu, D., Hai, T., Harding, H. P., Wang, X., Ron, D., Cavener, D. R., and Wek, R. C. (2004) Activating transcription factor 3 is integral to the eukaryotic initiation factor 2 kinase stress response. *Mol. Cell. Biol.* **24**, 1365–1377
49. Ye, J., Rawson, R. B., Komuro, R., Chen, X., Davé, U. P., Prywes, R., Brown, M. S., and Goldstein, J. L. (2000) ER stress induces cleavage of membrane-bound ATF6 by the same proteases that process SREBPs. *Mol. Cell* **6**, 1355–1364
50. Vacaru, A. M., Di Narzo, A. F., Howarth, D. L., Tsedensodnom, O., Imrie, D., Cinaroglu, A., Amin, S., Hao, K., and Sadler, K. C. (2014) Molecularly defined unfolded protein response subclasses have distinct correlations with fatty liver disease in zebrafish. *Dis. Model. Mech.* **7**, 823–835
51. Rouschop, K. M. A., van den Beucken, T., Dubois, L., Niessen, H., Bussink, J., Savelkouls, K., Keulers, T., Mujcic, H., Landuyt, W., Voncken, J. W., Lambin, P., van der Kogel, A. J., Koritzinsky, M., and Wouters, B. G. (2010) The unfolded protein response protects human tumor cells during hypoxia through regulation of the autophagy genes *MAP1LC3B* and *ATG5*. *J. Clin. Invest.* **120**, 127–141
52. B'chir, W., Maurin, A.-C., Carraro, V., Averous, J., Jousse, C., Muranishi, Y., Parry, L., Stepien, G., Fafournoux, P., and Bruhat, A. (2013) The eIF2α/ATF4 pathway is essential for stress-induced autophagy gene expression. *Nucleic Acids Res.* **41**, 7683–7699
53. He, C., Bartholomew, C. R., Zhou, W., and Klionsky, D. J. (2009) Assaying autophagic activity in transgenic GFP-Lc3 and GFP-Gabarap zebrafish embryos. *Autophagy* **5**, 520–526
54. Ylä-Anttila, P., Vihinen, H., Jokitalo, E., and Eskelinen, E.-L. (2009) Monitoring autophagy by electron microscopy in mammalian cells. *Methods Enzymol.* **452**, 143–164
55. Davies, R., Schuurman, A., Barker, C. R., Clothier, B., Chernova, T., Higginson, F. M., Judah, D. J., Dinsdale, D., Edwards, R. E., Greaves, P., Gant, T. W., and Smith, A. G. (2005) Hepatic gene expression in protoporphyic Fech mice is associated with cholestatic injury but not a marked depletion of the heme regulatory pool. *Am. J. Pathol.* **166**, 1041–1053
56. Magnus, I. A., Roe, D. A., and Bhutani, L. K. (1969) Factors affecting the induction of porphyria in the laboratory rat. Biochemical and photobiological studies using diethyl 1,4-dihydro-2,4,6-trimethyl-pyridine-3,5-dicarboxylate (DDC) as a porphyrogenic agent. *J. Invest. Dermatol.* **53**, 400–413
57. Gschnait, F., Konrad, K., Hönigsmann, H., Denk, H., and Wolff, K. (1975) Mouse model for protoporphyria. I. The liver and hepatic protoporphyrin crystals. *J. Invest. Dermatol.* **65**, 290–299
58. Rubinstein, A. L. (2003) Zebrafish: from disease modeling to drug discovery. *Curr. Opin. Drug Discov. Devel.* **6**, 218–223
59. Kaufman, C. K., White, R. M., and Zon, L. (2009) Chemical genetic screening in the zebrafish embryo. *Nat. Protoc.* **4**, 1422–1432
60. Plewinska, M., Thunell, S., Holmberg, L., Wetmur, J. G., and Desnick, R. J. (1991) delta-Aminolevulinate dehydratase deficient porphyria: identification of the molecular lesions in a severely affected homozygote. *Am. J. Hum. Genet.* **49**, 167–174
61. Van Steveninck, J., Boegheim, J. P., Dubbelman, T. M., and Van der Zee, J. (1988) The influence of porphyrins on iron-catalysed generation of hydroxyl radicals. *Biochem. J.* **250**, 197–201
62. MacDonald, D. M., Germain, D., and Perrot, H. (1981) The histopathology and ultrastructure of liver disease in erythropoietic protoporphyria. *Br. J. Dermatol.* **104**, 7–17
63. Komatsu, H., Sajima, Y., Imamura, K., Masuda, H., Yonei, Y., Dohmori, K., Kokutoh, M., Ishii, K., and Ishii, H. (2000) An ultrastructural study of the liver in erythropoietic protoporphyria. *Med. Electron Microsc.* **33**, 32–38

Received for publication October 18, 2015.
Accepted for publication January 6, 2016.